ISSN 1068-798X, Russian Engineering Research, 2016, Vol. 36, No. 9, pp. 774–780. © Allerton Press, Inc., 2016.
Original Russian Text © V.V. Bushuev, S.V. Evstafieva, V.V. Molodtsov, 2016, published in STIN, 2016, No. 3, pp. 7–14.

Control Loops of a Supply Servo Drive

V. V. Bushuev*, S. V. Evstafieva, and V. V. Molodtsov**

Stankin Moscow State Technical University, Moscow, Russia

**e-mail: busheck@yandex.ru*

***e-mail: v_molodtsov@mail.ru*

Abstract—The electric motor in a supply drive is analyzed. The model employed takes account of the motor's electrical and mechanical parameters and permits reproduction of the processes in the control loops of supply drives.

Keywords: servo motors, supply drives, mechatronics, mathematical model

DOI: 10.3103/S1068798X16090069

In the dynamic calculation, debugging, and diagnostics of supply drives, we lack mathematical models capable of describing the interaction of the mechanical and electrical components in the drive [1–3]. The main problem for machine-tool specialists is modeling of the drive's electrical component.

In the present work, we present a relatively simple model of the electromechanical component of a drive, including a motor and a feedback loop on the basis of experiments and simulation. The model qualitatively and quantitatively reproduces the processes in servo supply drives with satisfactory reliability [4].

We employ a Sinamics S120 (Siemens) electric drive, whose control system is integrated in a Simotion D435 controller (Fig. 1). The drive controls 1FT7046-5AF70-1FH0 and 1FK7061-7AF71-1FH0 motors. The built-in photoelectric sensors are used as the displacement sensors in the position-control loop. The drive's control system lacks special sensors for measurement of the motor speed. Information regarding the actual motor speed is obtained by differentiation of the signal from the position sensor. The basic parameters of the motors and the drive are presented in Tables 1 and 2, respectively. In Table 1, we adopt the following notation: J_Σ is the rotor's moment of inertia in braking; M_{rat} is the rated torque; $M_{to.max}$ is the maximum torque; J_{max} is the maximum current.

The diagnostic system employed is part of the software for the drives' control devices and the higher-level controller. This system permits qualitative and quantitative analysis of the drive characteristics without special equipment, with great diversity of the input diagnostic signals. For present purposes, attention is confined to the logarithmic amplitude–frequency characteristics and logarithmic phase–frequency characteristics of the drive loops, as well as their reactions to spikes in the control signal.

Simulation is based on Simulink software, which forms part of the MATLAB suite of programs. In simulation, the main problem is to select the simplest possible model of the drive's operating system, consisting of the motor and the controllable power source (frequency converter). Such a model was proposed in [4].

In Fig. 2a, we show the structure of two internal loops of the servo drive, including its operating system and feedback with respect to the motor emf, current, and speed. The notation for the model parameters is indicated in Fig. 2a: $T_e = L_e/R_e$ is the electromagnetic time constant of the stator winding; L_e and R_e are the inductance and resistance of the stator winding; K_{co} is the amplification factor of the frequency converter; K_m and K_e are electromechanical constants of the motor; $W_m(s)$ is the transfer function of the drive's mechanical component; τ_{cu} is the time constant of the pure

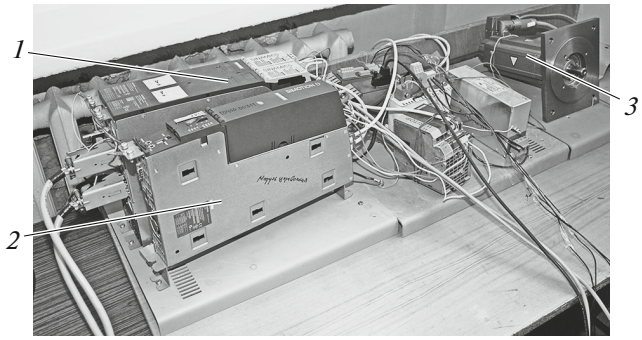

Fig. 1. Servo drive: (*1*) dc motor; (*2*) SINAMICS S120 drive; (*3*) SIMOTION D435 controller.

Table 1

Motor	Parameters						
	J_Σ, kg m^2	K_m, N m/A	L_e, H	R_e, Ω	M_{rat}, N m	$M_{cr.max}$, N m	J_{max}, A
1FT7046-5AF70-1FH0	0,000839	1.75	0.011	1.55	5.6	31	19
1FK7061-7AF71-1FH0	0.000374	1.0	0.02	0.74	5.4	17.3	17.5

* The rated speed for both motors is 3000 rpm.

delay component, taking account of the time for information transfer in the current loop.

In the control loops, we use standard PI regulators with transfer functions

$$W_{cr}(s) = K_{cr}\left(1+\frac{1}{T_{cr}s}\right) \text{ and } W_{sr}(s) = K_{sr}\left(1+\frac{1}{T_{sr}s}\right),$$

where K_{cr}, K_{sr} and T_{cr}, T_{sr} are the amplification factors and time constants for the current and speed regulators, respectively. The basic variables of the model are as follows: $\Omega_{sp}(s)$, $\Omega(s)$, and $\Omega_{me}(s)$ are the specified, effective, and measured motor speeds, respectively; $\Delta\Omega(s)$ is the discrepancy between the specified and measured speeds; $M(s)$ and $M_{dr}(s)$ are the motor torque and the drag torque, respectively. $U_{sp}(s)$ and $U(s)$ are the projections of the specified voltage and the effective voltage (the voltage applied to the motor windings) onto the q axis.

In Figs. 2b and 2c, we present the following model variables: $i_{sp}(s)$, $i(s)$, and $i_{me}(s)$ are the projections of the specified, effective, and measured current in the motor windings onto the q axis; $i_{sp}'(s)$ is the current specification from the speed regulator; $\Delta i(s)$ is the mismatch between the projections of the specified and measured current; $\Delta i_{sp}'(s)$ is the result of transformation of the mismatch signal by the component $W_{m1}(s)$.

Table 2

Motor	Parameters of SINAMICS S120 drive		
	K_{sr}, N ms/rad	K_{cr}, V/A	T_{cr}, ms
1FT7046-5AF70-1FH0	1.04	18.6	7
1FK7061-7AF71-1FH0	0.46	40	27

* The servo-drive parameters are as follows for both motors: K_{sd} = 1 V; $K_{por} = 382\ s^{-1}$; $\tau_c = 125$ μs; $\tau_0 = 1000$ μs; $T_{sr} = 1.31$ ms.

We show the structure of the position loop in Fig. 2d, where the notation for the model parameters is indicated: $W_{sr}(s)$ is the transfer function for the speed loop; τ_{po} is the time constant of the pure delay component, taking account of the time for information transfer between the controller modules; K_{por} is the amplification factor of the position regulator; $T_f = T_{sr}$ is the time constant of the filter in the speed-specification circuit.

The motor (Fig. 2a) is regarded as a sequence of aperiodic, proportional, and integrating components, with speed feedback. The frequency converter is described by a proportional component with the appropriate amplification factor. The time required

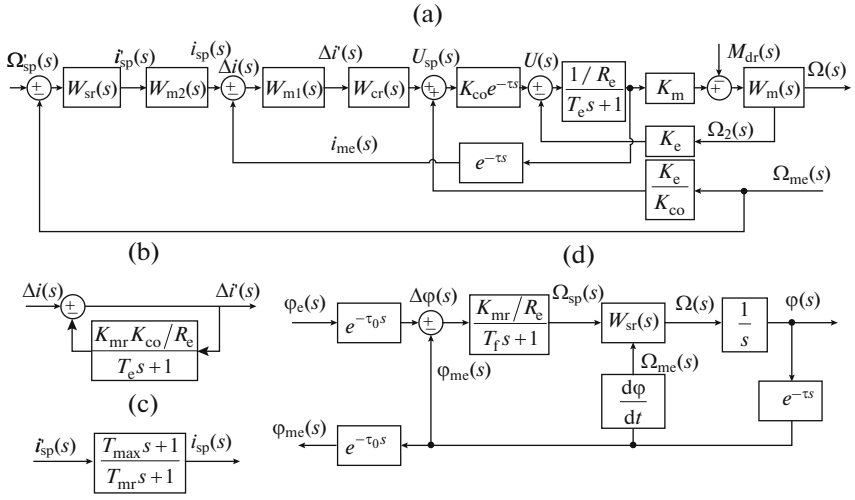

Fig. 2. Structure of the servo-drive model: (a) controllable drive; (b, c) components of the model; (d) position loop.

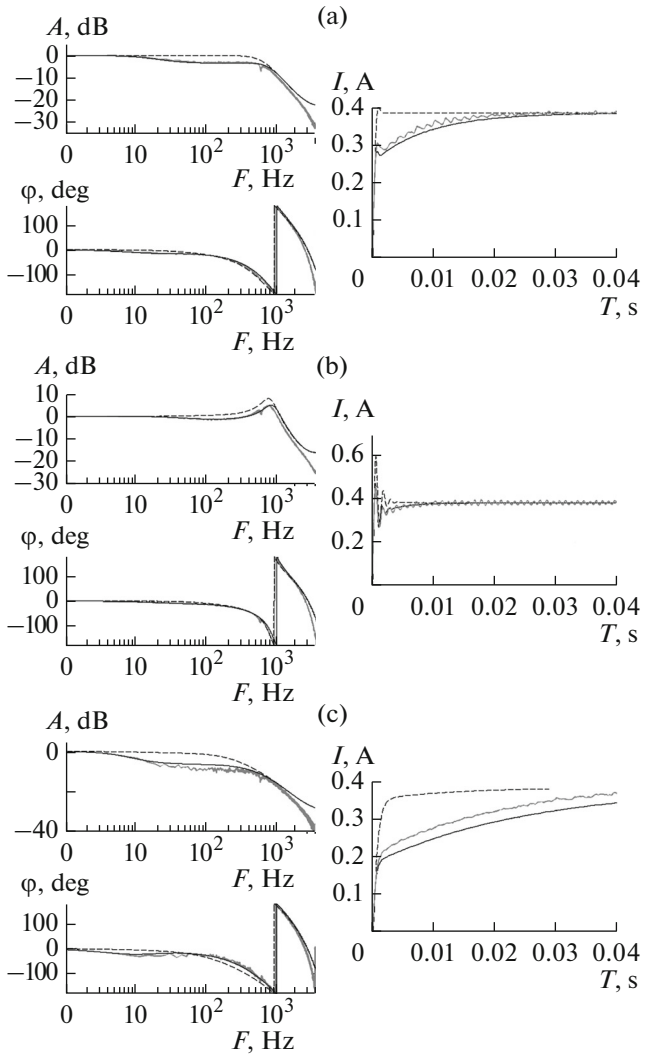

Fig. 3. Logarithmic amplitude–frequency characteristics and logarithmic phase–frequency characteristics of the transfer function $W_{clo}(s) = i(s)/i_{sp}(s)$ and the reaction I of the current loop for a servo drive with a 1FT7046-5AF70-1FH0 motor to a spike in the control signal with variation in the regulator settings: K_{cr} and T_{cr} (a); $2K_{cr}$ and $0.5T_{cr}$ (b); $0.5K_{cr}$ and $2T_{cr}$ (c).

for information transmission is represented by pure delay components with unit amplification factor. In the research, their positions are determined, and quantitative estimates are obtained for the delay in the system. The delay corresponds to the operating time required for the current, speed, and position control loops [4].

The delay slows down the transmission of the necessary information regarding the state of the system to the regulators and the control signal from the regulators to the object. That impairs the dynamic characteristics of the system and leads to stability loss at a certain value of the delay.

Since the current loop is astatic with respect to the specification, a positive feedback loop is created for the emf supplied to the input of the frequency converter with the control signal (Fig. 2a) [5]. To measure the speed, there is no need to use another sensor, since the derivative of the signal from the position sensor may be used to ensure speed feedback. Siemens has been using this method of compensating the motor emf in its drives since the end of the 1960s [6].

In order to assess the sensitivity of the drive's control loops to adjustment of the regulator settings, we investigate their characteristics with different values of the amplification factors and the time constants of integration for the current and speed regulators. (Specifically, the values employed are twice and half as large as the tabular values.) We conduct experiments and computer experiments with different combinations of K_{cr} and T_{cr}. The speed loop is investigated analogously. Tables 1 and 2 present the baseline values of the model parameters and the regulator settings for a real drive.

The logarithmic amplitude–frequency characteristics and logarithmic phase–frequency characteristics and the reactions to spikes in the input signal mainly determine the dynamic properties of the system. In Figs. 3 and 4, we show the corresponding characteristics of the current and speed loops for a servo drive with a 1FT7046-5AF70-1FH0 motor obtained by measurement (gray lines) and calculation (black lines).

The current loop of the real drive has somewhat better dissipative properties than are seen in the model (as is evident from the dashed lines in Fig. 3). That may be attributed to the special hybrid model in the current and speed loops, the position, structure, and parameters of whose components are hidden from the user. We may suppose that the model is intended to compensate the influence of the time delays during information transmission in the current loop on its dynamics, to ensure the required quality of the transient processes during control of the motor torque, and to compensate the influence of the large time constants of the current loop on the dynamic processes in the speed and position loops.

Analysis of existing methods used to compensate the influence of the pure delay components and the experimental characteristics of the current and speed loops indicate that the hybrid model includes two components $W_{m1}(s)$ and $W_{m2}(s)$, the first of which is in the control channel of the current loop, while the second is in the control channel of the speed loop (Fig. 2a) [4].

The transfer function $W_{m1}(s)$ is similar to that of a current loop with a proportional regulator $0 \le K_{mr} \le K_{cr}$ in the absence of an integral channel. In Fig. 2b, we show its structure. By selecting the amplification factor of the regulator in the internal model, we may significantly improve the dynamic characteristics of the

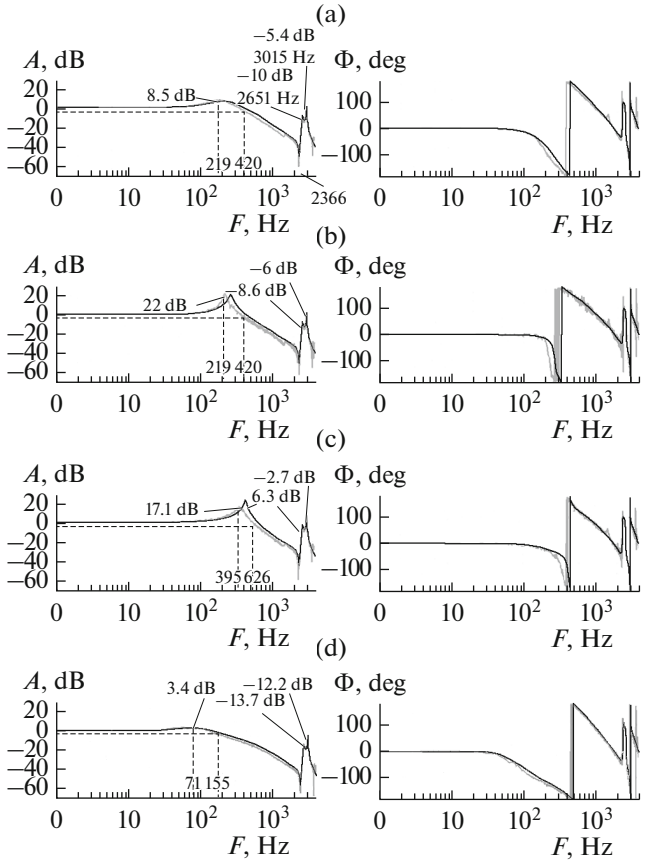

Fig. 4. Logarithmic amplitude–frequency characteristics and logarithmic phase–frequency characteristics of the transfer function $W_{slo}(s) = \Omega(s)/\Omega_{sp}(s)$ for the speed loop of a servo drive with a 1FT7046-5AF70-1FH0 motor with variation in the regulator settings: K_{sr} and T_{sr} (a); K_{sr} and $0.5T_{sr}$ (b); $2K_{sr}$ and $0.5T_{sr}$ (c); $0.5K_{sr}$ and $2T_{sr}$ (d).

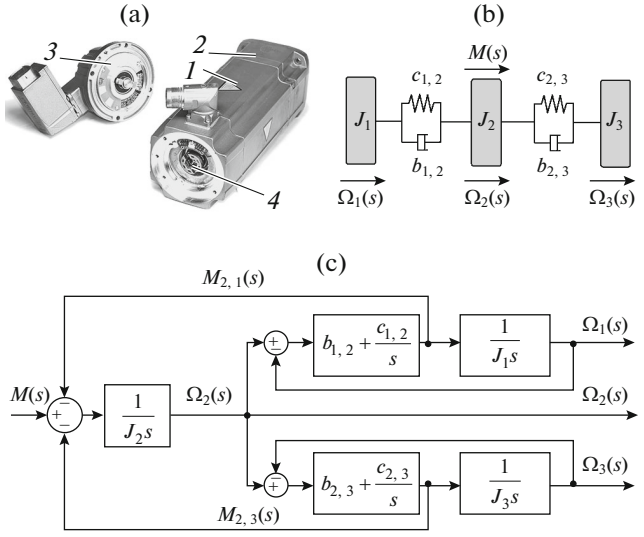

Fig. 5. External appearance of the 1FT7046-5AF70-1FH0 motor *1* with the brake *2*, position sensor *3* and elastic coupling *4* (a); structure of motor (b); and mathematical model of its mechanical part (c).

current loop in the specification channel. The logarithmic amplitude–frequency characteristic, logarithmic phase–frequency characteristic, and reaction of the current loop to spikes in the input signal are shown by solid black lines in Figs. 3 and 4. Comparison of the results indicates that, with the given settings, the output characteristics of the model and the actual system are consistent.

The transfer function $W_{m2}(s)$ is shown in Fig. 2c. It is intended for compensation of the large time constants T_{cr} in the numerator and T_{max} in the denominator of the current loop.

The frequency characteristics of the speed loop have a more complex spectral composition (Fig. 4). Besides the pole in the range 70–360 Hz, where the eigenfrequency and amplitude of the output signal depend on the change in settings of the speed regulator, we also note a zero at 2366 Hz and poles at 2651 and 3015 Hz. These are outside the transmission band of the speed loop, which is 626 Hz with doubling of the amplification factor (Fig. 4c); their eigenfrequencies do not depend on the change in regulator parameters.

However, the height of the resonant peaks at 2651 and 3015 Hz increases with increase in the amplification factor or decrease in the regulator's time constant. The increase in amplitude at 3015 Hz is particularly significant (Fig. 4c). With simultaneously doubling of K_{sr} and decrease in T_{cr}, the speed loop becomes unstable.

Analysis of information regarding the motor design (Fig. 5a) indicates that the source of the resonant peaks in the upper part of the frequency range is mechanical. The 1FT7046-5AF70-1FH0 motor is of modular structure, with three basic components: the motor itself (*1*), the brake (*2*), and the position sensor (*3*). The rotor and the mobile parts of the brake are attached to the motor shaft, to which the sensor shaft is connected by means of an elastic coupling (*4*). The motor shaft is assumed to be nonrigid.

According to the analysis, the minimum model of the motor's mechanical component required to describe resonant phenomena may be represented as a three-component chain (Fig. 5b). In the model, distributed inertial, elastic, and dissipative characteristics of the drive components are taken into account by three rotating point masses (according to the number of eigenfrequencies) and the elastic and dissipative

connections between them. The model may be written in the form

$$\left.\begin{aligned} J_1 s^2 \varphi_1(s) &= (b_{1,2}s + c_{1,2})[\varphi_2(s) - \varphi_1(s)]; \\ J_2 s^2 \varphi_2(s) &= M(s) - (b_{1,2}s + c_{1,2})[\varphi_2(s) - \varphi_1(s)] \\ &\quad - (b_{2,3}s + c_{2,3})[\varphi_2(s) - \varphi_3(s)]; \\ J_3 s^2 \varphi_3(s) &= (b_{2,3}s + c_{2,3})[\varphi_2(s) - \varphi_3(s)], \end{aligned}\right\}. \quad (1)$$

Here J_1 is the reduced moment of inertia of the section of the motor shaft with the brake; J_2 is the reduced moment of inertia of the section of the motor shaft with the rotor; J_3 is the reduced moment of inertia of the sensor shaft; $c_{i,k}$ and $b_{i,k}$ are the torsional rigidity and damping coefficient of the corresponding structural element, respectively; $M(s)$ is the torque on the motor's rotor due to the stator; and $\varphi_i(s)$ is the twist angle of motor element i at the positions of the corresponding reduced masses.

If we replace $\varphi_i(s)$ by the variable components of the drive elements' speeds—that is, $\varphi_i(s) = \Omega_i(s)/s$—we may write Eq. (1) in form a convenient for describing the structure of the model of the drive's mechanical component

$$\left.\begin{aligned} J_1 s\Omega_1(s) &= (b_{1,2} + c_{1,2}/s)[\Omega_2(s) - \Omega_1(s)]; \\ J_2 s\Omega_2(s) &= M(s) - (b_{1,2} + c_{1,2}/s)[\Omega_2(s) - \Omega_1(s)] \\ &\quad - (b_{2,3} + c_{2,3}/s)[\Omega_2(s) - \Omega_3(s)]; \\ J_3 s\Omega_3(s) &= (b_{2,3} + c_{2,3}/s)[\Omega_2(s) - \Omega_3(s)]. \end{aligned}\right\}. \quad (2)$$

In Fig. 5c, we show the structure corresponding to Eq. (2).

Solving Eq. (2), we determine the variable speed components of the second and third masses, corresponding to the motor's rotor and sensor

$$\Omega_2(s) = \frac{(J_1 s^2 + b_{1,2}s + c_{1,2})(J_3 s^2 + b_{2,3}s + c_{2,3})}{G(s)} M(s); \quad (3)$$

$$\Omega_3(s) = \frac{(J_1 s^2 + b_{1,2}s + c_{1,2})(b_{2,3}s + c_{2,3})}{G(s)} M(s), \quad (4)$$

where

$$\begin{aligned} G(s) &= J_2 s(J_1 s^2 + b_{1,2}s + c_{1,2})(J_3 s^2 + b_{2,3}s + c_{2,3}) \\ &\quad + J_1 s(b_{1,2}s + c_{1,2})(J_3 s^2 + b_{2,3}s + c_{2,3}) \\ &\quad + J_3 s(J_1 s^2 + b_{1,2}s + c_{1,2})(b_{2,3}s + c_{2,3}). \end{aligned}$$

The formulas obtained have a common denominator $G(s)$, known as the characteristic polynomial, one of whose roots is zero. The zero root corresponds to displacement of the unattached system as a rigid body. The numerators in Eqs. (3) and (4) determine the zeros of the variable speed components. The peaks and troughs corresponding to the complex-conjugate poles and zeros of the function $W_3(j\omega) = \Omega_3(j\omega)/M(j\omega)$ may be observed on the experimental frequency characteristics of the speed loop (Fig. 4).

Since the rotating part of the motor is a slightly damped mechanical system, we assume that the damping forces have little influence on its eigenfrequencies and the forms of vibration. In that case, the damping may be neglected in determining the eigenfrequencies [7]. Discarding the zero root and assuming that $b_{1,2} = b_{2,3} = 0$, we write the equations for the nonzero eigenvalues of $W_3(s)$ in the form

$$\begin{aligned} s^4 + \left[\left(\frac{1}{J_1} + \frac{1}{J_2}\right)c_{1,2} + \left(\frac{1}{J_2} + \frac{1}{J_3}\right)c_{2,3}\right]s^2 \\ + \frac{J_1 + J_2 + J_3}{J_1 J_2 J_3} c_{1,2}c_{2,3} = 0 \end{aligned}; \quad (5)$$

$$s^2 + \frac{c_{1,2}}{J_1} = 0. \quad (6)$$

After the substitution $s = j\omega$, we obtain

$$\begin{aligned} \omega^4 - \left[\left(\frac{1}{J_1} + \frac{1}{J_2}\right)c_{1,2} + \left(\frac{1}{J_2} + \frac{1}{J_3}\right)c_{2,3}\right]\omega^2 \\ + \frac{J_1 + J_2 + J_3}{J_1 J_2 J_3} c_{1,2}c_{2,3} = 0 \end{aligned}; \quad (7)$$

$$\omega^2 - \frac{c_{1,2}}{J_1} = 0. \quad (8)$$

For biquadratic algebraic Eq. (7), the relations between the roots and the coefficients are established by means of Vieta's formulas [8]. Assuming that the roots are known, we may write a system of equations for the coefficients in Eqs. (7) and (8)

$$\left.\begin{aligned} \left(\frac{1}{J_1} + \frac{1}{J_2}\right)c_{1,2} + \left(\frac{1}{J_2} + \frac{1}{J_3}\right)c_{2,3} &= p_1 + p_2; \\ \frac{J_1 + J_2 + J_3}{J_1 J_2 J_3} c_{1,2}c_{2,3} &= p_1 p_2; \\ \frac{c_{1,2}}{J_1} &= z; \\ J_1 + J_2 + J_3 &= J_\Sigma, \end{aligned}\right\}, \quad (9)$$

where $p_1 = \omega_1^2$, $p_2 = \omega_2^2$, and $z = \omega_0^2$ are eigenvalues ($z < p_1 < p_2$) corresponding to the complex-conjugate poles and zeros of the function $W_3(j\omega)$; J_Σ is the rotor moment of inertia for the motor with the brake and sensor (Table 1).

If the unknowns in Eq. (9) are J_1, J_2, J_3, $c_{1,2}$, and $c_{2,3}$, it may be regarded as a system of four algebraic equations with five unknowns. Eliminating the variables $c_{1,2}$, $c_{2,3}$, and J_3, we obtain the equation

$$\left(\frac{p_1 p_2}{z^2} - \frac{1}{J_2/J_\Sigma}\right)J_1/J_\Sigma = \left(1 - \frac{p_1}{z}\right)\left(1 - \frac{p_2}{z}\right) \quad (10)$$

with two variables

$$0 < J_1/J_\Sigma < 1 \text{ and } 0 < J_2/J_\Sigma < 1.$$

Selecting J_2/J_Σ as the free variable, we write the solution in the form

$$J_1/J_\Sigma = \frac{(1 - z/p_1)(1 - z/p_2)}{J_2/J_\Sigma - \dfrac{z^2}{p_1 p_2}} J_2/J_\Sigma.$$

The region of permissible values of this solution is found by taking into account that $J_3 > 0$. Hence, $J_1/J_\Sigma + J_2/J_\Sigma < 1$. If we substitute the expression $J_1/J_\Sigma = 1 - J_2/J_\Sigma$ into Eq. (10), we obtain a quadratic equation

$$\left(\frac{J_2}{J_\Sigma}\right)^2 - \left(\frac{z}{p_1} + \frac{z}{p_2}\right)\frac{J_2}{J_\Sigma} + \frac{z^2}{p_1 p_2} = 0.$$

Its solution yields the region of permissible values of the rotor's moment of inertia: $z/p_2 < J_2/J_\Sigma < z/p_1$. In Fig. 6a, we plot J_1/J_Σ and J_3/J_Σ against J_2/J_Σ.

In Figs. 6b–6d, we present the results of approximation for three sets of model parameter values, close to the minimum and maximum permissible values of J_2 and the maximum value of J_3, as shown in Table 3, where $\zeta_{i,j}$ are dimensionless damping factors

$$\zeta_{1,2} = \frac{b_{1,2}}{2\sqrt{c_{1,2}J_1}} \text{ and } \zeta_{2,3} = \frac{b_{2,3}}{2\sqrt{c_{2,3}J_3}}.$$

Analysis of the results indicates that the best approximation to the experimental frequency characteristics is obtained on the basis of the model parameter values close to the minimum and maximum permissible values of J_2. On the basis of data regarding the moments of inertia of the brake and the damping coefficients, as well as the fact that the elastic coupling between the motor and the sensor is made of plastic, we conclude that the actual structure corresponds to the case with $J_2/J_\Sigma = 0.791$. The solid black curves in Fig. 4 show the frequency characteristics calculated for this case.

Comparison indicates that the characteristics of the model's speed loop are in good qualitative and quantitative agreement with the characteristics of the real drive, with variation in the amplification factors and time constants of the regulators.

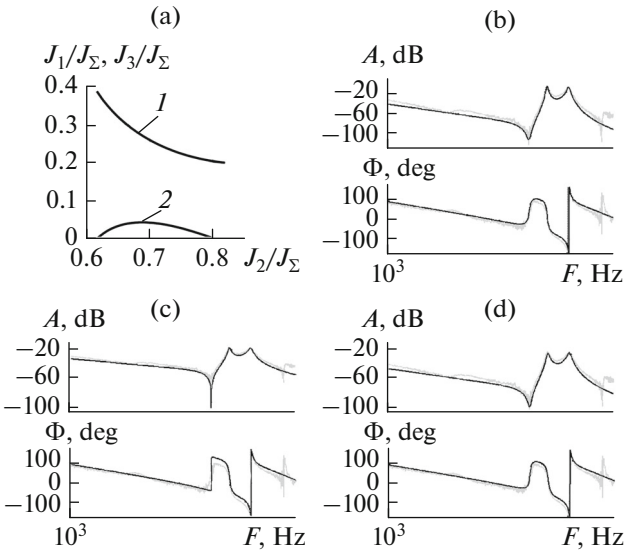

Fig. 6. Relation between the moments of inertia and approximation of the frequency characteristics of the speed loop with the tabular values of K_{sr} and T_{sr}: dependence of J_1/J_Σ and J_3/J_Σ on J_2/J_Σ (a); $J_2/J_\Sigma = 0.62$ (b); $J_2/J_\Sigma = 0.687$ (c); and $J_2/J_\Sigma = 0.791$ (d).

Analysis of the model's output characteristics demonstrates that the resonant phenomena in the motor's mechanical component at 3015 Hz are related to the increase in intensity of sensor vibrations relative to the motor's rotor. However, these phenomena do not explain the stability loss of the drive with simultaneous doubling of K_{sr} and decrease in T_{cr} with respect to the tabular values. The model of the speed loop in which the mechanical component is represented by an absolutely rigid body with moment of inertia $J_\Sigma = J_1 + J_2 + J_3$ also becomes unstable with the given speed-regulator settings [4].

In Fig. 2d, the position loop has the following model parameters: $\varphi_{sp}(s)$, $\varphi_{sp}'(s)$, $\varphi(s)$, $\varphi_{me}(s)$, and $\varphi_{ob}(s)$, which are, respectively, the specified positional angle of the motor's rotor, the specified value taking account of the delay in information transmission, the effective value, the measured value, and the observed value. On account of the time delay τ_0 in the open section of the position loop, the logarithmic phase–frequency characteristic of the observed signal has an

Table 3

J_2/J_Σ	$J_1 \times 10^{-4}$	$J_2 \times 10^{-4}$	J_3	$c_{1,2}$	$c_{2,3}$	$b_{1,2}/\xi_{1,2}$	$b_{2,3}/\xi_{2,3}$
0.62	3.143	5.202	$4.5\ 10^{-06}$	70575	1272	0.1/0.011	0.001/0.0066
0.687	2.272	5.763	$3.55\ 10^{-05}$	51030	11057	0.001/0.0001	0.025/0.002
0.791	1.699	6.636	$5.5\ 10^{-06}$	38147	1979	0.04/0.0079	0.003/0.0144

* Damping coefficients/dimensionless attenuation coefficients.

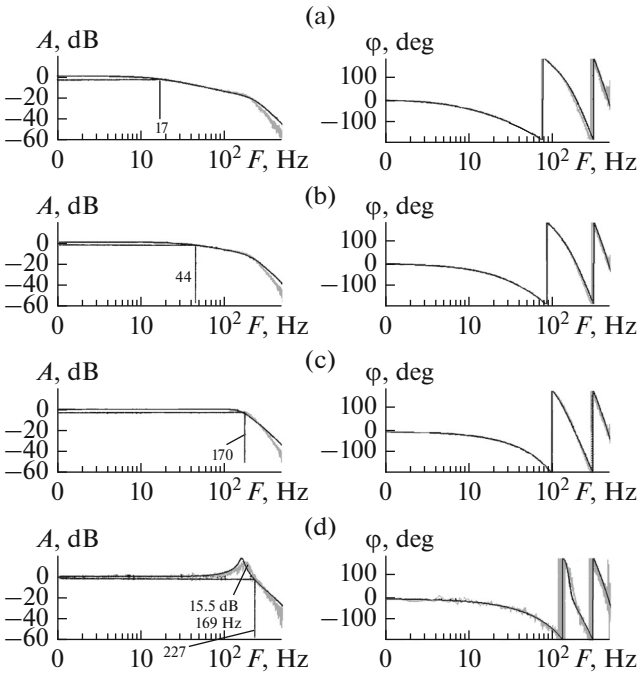

Fig. 7. Logarithmic amplitude–frequency characteristics and logarithmic phase–frequency characteristics of the transfer function $W_{polo}(s) = \varphi_{ob}(s)/\varphi_{sp}(s)$ for the position loop of the servo drive with a 1FT7046-5AF70-1FH0 motor, with different amplification factors of the position loop and tabular values of the speed-loop coefficients: $K_{por} = 95\ s^{-1}$ (a), $191\ s^{-1}$ (b), $382\ s^{-1}$ (c), and $764\ s^{-1}$ (d).

additional phase shift not present in the effective and measured signals [4].

In Fig. 7, we present the logarithmic phase–frequency characteristics of the position loop for a drive with a 1FT7046-5AF70-1FH0 motor, for different values of the amplification factors in the loop. (Specifically, the values employed are twice and one quarter as large as the tabular values.) The light lines show the measured characteristics, while the dark lines show the calculated characteristics.

We see that, with eightfold increase in the amplification factor, from 95 to 764 s^{-1}, the drive's transmission band increases from 17 to 227 Hz. However, when the amplification factor is larger than 382 s^{-1}, we note the formation of a resonant peak, which is 15.5 dB at 764 s^{-1}. The resonant phenomena in the loop limit the possible increase in the speed.

Comparison of the graphs in Fig. 7 indicates that the characteristics of the model's position loop are in good qualitative and quantitative agreement with the characteristics of the real drive.

Analogous analysis of a servo drive with a 1FK7061-7AF71-1FH0 motor leads to similar results, if we take account of its physicochemical characteristics and structure.

CONCLUSIONS

(1) The processes in the control loops of supply drives may be qualitatively and quantitatively reproduced, with satisfactory reliability, by relatively simple description of the servo drive on the basis of a model of the dc motor.

(2) The informational delays have a significant influence on the dynamic processes in the control loops and must be taken into account in drive design.

(3) The actual drive is more robust than a linear mathematical model. That may be attributed to the action of specialized modules hidden from the user, whose structure is known only to the Siemens company.

(4) The elastic properties of the motor's mechanical component appear in the high-frequency range of the dynamic characteristics, outside the transmission band of the speed loop. In certain conditions, the resonant phenomena associated with mechanical vibrations in the drive may prevent increase in the amplification factors of the speed and position loops to the required values. However, despite its importance, this problem remains to be adequately studied.

ACKNOWLEDGMENTS

Financial support was provided by the Ministry of Education and Science of the Russian Federation (project no. 9.1429.2014/K).

REFERENCES

1. Molodtsov, V.V., Construction and calculation of the displacing drive of CNC machines with the screw-nut rolling motion, *Spravochnik. Inzh. Zh.*, 2007, no. 1, suppl.
2. Sabirov, F.S. and Savinov, S.Y., Diagnostics and control of the accuracy of axis drives for automatically controlled multicoordinate metal cutting machines, *Meas. Tech.*, 2011, vol. 54, no. 8, pp. 879–882.
3. Idrisova, Yu.V., Kudoyarov, R.G., and Fetsak, S.I., Operative diagnostics of technical status of the drives of metal-processing machines, *Vestn. Ufim. Gos. Aviats. Tekhn. Univ.*, 2012, vol. 16, no. 4 (49), pp. 113–119.
4. Evstafieva, S.V. and Molodtsov, V.V., Simulation tracking feed drive for modern machine-tools with CNC, *Mekhatron., Avtom., Uprav.*, 2010, no. 9, pp. 37–44.
5. Mikhailov, O.P., *Dinamika elektromekhanicheskogo privoda metallorezhushchikh stankov (The Dynamics of an Electromechanical Drive of Metal-Cutting Machines)*, Moscow: Mashinostroenie, 1989.
6. Sokolovskii, G.G., *Elektroprivody peremennogo toka s chastotnym regulirovaniem: uchebnik dlya studentov vysshikh uchebnykh zavedenii (AC Electrodrives with Frequency Regulation: Manual for Higher Education Students)*, Moscow: Akademiya, 2006.
7. Weaver, Jr., W., Timoshenko, S.P., and Young, D.H., *Vibration Problems in Engineering*, New York: Wiley, 1990.
8. Kurosh, A.G., *Kurs vysshei algebry (The Lectures on Higher Algebra)*, Moscow: Nauka, 1968.

Translated by Bernard Gilbert